AIP | Review of Scientific Instruments

Invited Article: Coherent imaging using seeded free-electron laser pulses with variable polarization: First results and research opportunities

F. Capotondi, E. Pedersoli, N. Mahne, R. H. Menk, G. Passos et al.

Citation: Rev. Sci. Instrum. **84**, 051301 (2013); doi: 10.1063/1.4807157
View online: http://dx.doi.org/10.1063/1.4807157
View Table of Contents: http://rsi.aip.org/resource/1/RSINAK/v84/i5
Published by the American Institute of Physics.

Invited Article: Coherent imaging using seeded free-electron laser pulses with variable polarization: First results and research opportunities

F. Capotondi,[1] E. Pedersoli,[1] N. Mahne,[1] R. H. Menk,[1] G. Passos,[1,a)] L. Raimondi,[1] C. Svetina,[1] G. Sandrin,[1] M. Zangrando,[1,2] M. Kiskinova,[1,b)] S. Bajt,[3] M. Barthelmess,[3] H. Fleckenstein,[3] H. N. Chapman,[3] J. Schulz,[4] J. Bach,[5] R. Frömter,[5] S. Schleitzer,[6] L. Müller,[6] C. Gutt,[6] and G. Grübel[6]

[1]*FERMI, Elettra-Sincrotrone Trieste, SS 14 - km 163.5, 34149 Basovizza, Trieste, Italy*
[2]*CNR, Istituto Officina dei Materiali - TASC, SS 14 - km 163.5, 34149 Basovizza, Trieste, Italy*
[3]*CFEL-DESY, Notkestraße 85, 22607 Hamburg, Germany*
[4]*European XFEL GmbH, Albert-Einstein-Ring 19, 22761 Hamburg, Germany*
[5]*Universität Hamburg, Institut für Angewandte Physik, 20355 Hamburg, Germany*
[6]*DESY, Notkestraße 85, 22607 Hamburg, Germany*

(Received 16 January 2013; accepted 6 May 2013; published online 29 May 2013)

FERMI@Elettra, the first vacuum ultraviolet and soft X-ray free-electron laser (FEL) using by default a "seeded" scheme, became operational in 2011 and has been opened to users since December 2012. The parameters of the seeded FERMI FEL pulses and, in particular, the superior control of emitted radiation in terms of spectral purity and stability meet the stringent requirements for single-shot and resonant coherent diffraction imaging (CDI) experiments. The advantages of the intense seeded FERMI pulses with variable polarization have been demonstrated with the first experiments performed using the multipurpose experimental station operated at the diffraction and projection imaging (DiProI) beamline. The results reported here were obtained with fixed non-periodic targets during the commissioning period in 2012 using 20–32 nm wavelength range. They demonstrate that the performance of the FERMI FEL source and the experimental station meets the requirements of CDI, holography, and resonant magnetic scattering in both multi- and single-shot modes. Moreover, we present the first magnetic scattering experiments employing the fully circularly polarized FERMI pulses. The ongoing developments aim at pushing the lateral resolution by using shorter wavelengths provided by double-stage cascaded FERMI FEL-2 and probing ultrafast dynamic processes using different pump-probe schemes, including jitter-free seed laser pump or FEL-pump/FEL-probe with two color FEL pulses generated by the same electron bunch. [http://dx.doi.org/10.1063/1.4807157]

I. INTRODUCTORY REMARKS

Advances in microscopy techniques based on X-rays provided by brilliant light sources such as synchrotrons and compact laboratory X-ray lasers, have opened unprecedented opportunities to explore the properties of the matter with nm spatial resolution.[1–3] The attractiveness of X-ray microscopy approaches is that the specific interactions of X-rays with matter, namely, absorption and scattering, provide chemical and morphology sensitivity. In addition, the X-ray penetration power allows examination of samples too thick for electron microscopes and implementing 3D imaging as well. Historically, the major key issue for both "classical" lens-based X-ray microscopes, full-field imaging and scanning, has been the fabrication of optical elements for improving the X-rays focusing. Today the lens-based X-ray microscopes have almost reached the resolution limit of few tens of nm, also imposed by aberrations, depth-of-field range and radiation damage considerations.

Undoubtedly, the great advantage of lens-based X-ray microscopy in providing direct and simultaneous structure-composition information will continue to play a very important role in modern science and nano-technology by broadening the application fields. However, the desire to push further the lateral resolution to the wavelength dependent diffraction limit has stimulated the growing interest to another "unconventional" form of microscopy based on X-ray scattering, namely Coherent Diffraction Imaging (CDI), also known as lensless X-ray microscopy.[4–7] The principle of CDI is based on the interference effects in the coherent X-ray scattering of object charge-distribution that gives rise to a characteristic "speckle pattern," which encodes the object shape and nanostructure. The CDI can be regarded as a holography without a reference beam so the main obstacle for retrieval of the object's real-space image from the speckles is to recover the missing information about the phase of the scattered wavefront, which has been solved by combining the oversampling method with iterative algorithms. Since the X-ray scattering is element specific (there is an abrupt change in the absorption cross section and scattering phase at the inner shell electron resonances), chemical contrast can be gained by performing resonant CDI experiments by selecting proper photon energies.[8,9] In addition, resonant CDI

a)Present address: RAL, STFC, Didcot, Harwell, Oxford OX11 0QX, United Kingdom.
b)Author to whom correspondence should be addressed. Electronic mail: maya.kiskinova@elettra.trieste.it.

from magnetic materials using polarized X-rays provides information about magnetic spin distribution and orientation.[10] Today, about a decade after, the first CDI results were obtained using synchrotron light,[4] and later-on using table-top laser,[11–13] CDI has reached a mature stage as an attractive and reliable method with applications in many domains of material and life sciences. It should be noted that in parallel, several holographic approaches with a spatially separated reference wave have also been used[14] and in this paper, results using Fourier Transform Holography (FTH) are reported as well. FTH has advantages for strongly absorbing samples using soft X-rays since anomalous scattering at resonances makes phase retrieval in resonant-CDI more difficult.

The high degree of coherence, high intensity, and femtosecond pulse duration of VUV and X-ray Free Electron Lasers (FELs), also called 4th generation synchrotrons, have opened unprecedented opportunities for CDI[4] and FTH[14] experiments. In particular, the FELs have pushed up the CDI time resolution, also called 4th imaging dimension, since compared to the most advanced pulse slicing 3rd generation synchrotrons, the FEL peak brightness is at least two orders of magnitude higher. As has already been demonstrated by the recent CDI and holography experiments at FLASH and LCLS, an image of a non-periodic object can be recorded using a single sub 100 fs FEL pulse. This has made possible to image radiation sensitive samples on time scales shorter than the onset of radiation damage and enabled a revolutionary step in accessing ultrafast phenomena in matter on fs time scales and nm length scales.[15–17] It should be noted that compact laser technology has also made significant progress but still extremely short fs pulses with high brightness are limited to UV/visible wavelengths.[12,13]

The three FEL sources, namely FLASH in Germany,[18] LCLS in USA,[19] and SACLA in Japan,[20] are based on the process of Self Amplification of Spontaneous Emission (SASE), which gives access to very high pulse intensities and ultrashort pulse lengths but undesired properties of the SASE-based FELs are uncontrollable spikes in the temporal profile and a jitter in photon energy due to the start-up noise involved in the SASE process. For instance, the SASE radiation does not have sufficient temporal coherence for performing jitter-free time-resolved resonant CDI experiments and a monochromator is needed for the experiments. In order to overcome the limitations imposed by the SASE-FEL shot-to-shot fluctuations and to obtain fully coherent FEL pulses, different seeding schemes are under development and very recently self-seeding has successfully been demonstrated for the hard X-ray regime at the LCLS.[21]

FERMI@Elettra is the first VUV-soft X-ray FEL based on the high-gain harmonic generation seeding scheme for amplification of the photon avalanche. In this scheme, the electron bunch is seeded with an external laser pulse in the UV regime[22,23] allowing full control of the wavelength and bandwidth of the FERMI FEL pulses by varying the parameters of the seed. A remarkable advantage is the preservation of the seed's temporal coherence in the emitted radiation, which results in FEL pulses with a narrow Gaussian-like wavelength profile. The superior control of emitted radiation in terms of spectral purity and stability of seeded FEL pulses allows very fine tuning of the wavelength to a selected absorption edge, which as noted above is a stringent requirement for resonant CDI experiments.[8–10] FERMI@Elettra also is the first FEL using APPLE-type undulators that provide full polarization control of the radiation, which is of pivotal importance, e.g., for magnetic scattering experiments.

Here, we report the first results of CDI, FTH, and resonant magnetic scattering experiments using a dedicated experimental station at the Diffraction and Projection Imaging (DiProI) beamline, designed to make use of the coherence properties, shot-to-shot temporal and energy stability, tunability and variable polarization of the narrow-bandwidth FERMI pulses.[24–26]

II. EXPERIMENTAL

During the DiProI first experiments the FERMI FEL-1[22,23] was still operated in its commissioning phase without the fine-control of the pulse duration. The beam parameters of FERMI FEL-1 available during our experiments are summarized in Table I.

Figure 1(a) shows a layout of the DiProI beamline (red-line), where the multipurpose experimental station is located. The main diagnostic tools and beamline components are: (i) a spectrometer, providing on-line shot-by-shot information of the pulse intensity and spectral purity; (ii) beam attenuators, a gas cell, and aluminum filters; (iii) split-delay line for FEL pump-FEL probe time correlation experiments (to be commissioned in 2013); and (iv) Kirkpatrick-Baez (K-B) focusing mirror system. The high spectral purity of the seeded FERMI beam is a great advantage, since it avoids efficiency losses imposed by the use of a monochromator. The most important parameters for CDI experiments are the beam coherence, and flexible and variable beam dimensions keeping the spot position on the specimen, which can be secured having reliable transport and focusing optical elements. The performance of the focusing optics should ensure to match the focal spot size to the sample size (down to a few μm), to illuminate larger or smaller areas to reduce or increase the fluence on the sample, in order to optimize the signal level and reduce the radiation damage. In addition, to meet the requirements

TABLE I. FERMI FEL-1 key parameters relevant to the present experiments.

Wavelength range	20–32.5 nm
Electron beam energy	1.2 GeV
Bunch charge	~500 pC
Electron beam size (rms)	~150 μm
Repetition rate	10 Hz[a]
Pulse energy	5–30 μJ[b]
Photons per pulse @ 32.5 nm	~5×10^{12}
Pulse duration (calculated[22]) @ 32.5 nm	~85 fs
Photon energy bandwidth (rms) @ 32.5 nm	~20 meV
Photon beam divergence @ 32.5 nm	~40 μrad
Polarization	linear and circular

[a]Repetition rate will be increased to 50 Hz in 2013.
[b]The pulse energy has already reached 100 μJ.

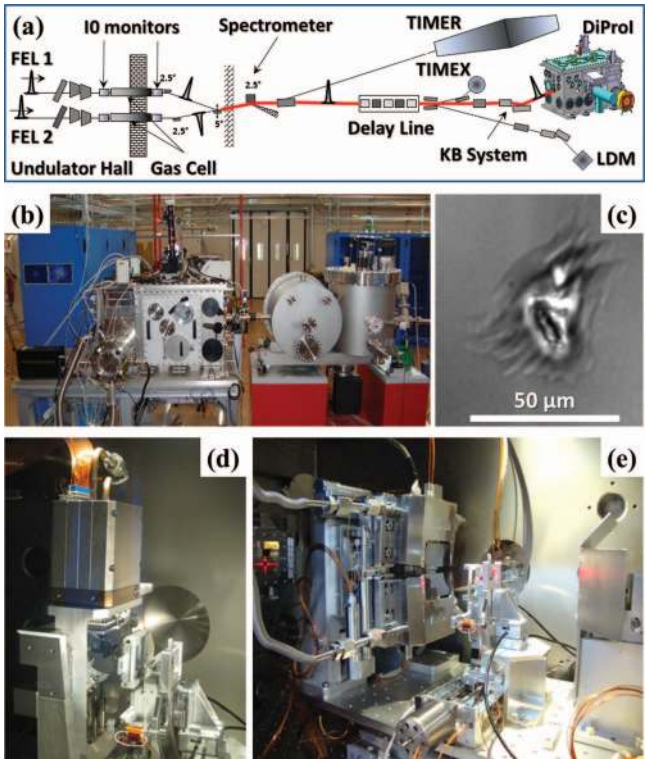

FIG. 1. (a) Beamline layout. (b) DiProI end-station connected to the double chamber hosting the K-B focusing system. (c) Optical microscope image of an ablated crater, created in a PMMA sample by the focused beam. (d) Indirect multi-layer mirror-CCD detection system. (e) X-CAM direct detection system.

of the actual experiment, the beam intensity can be varied by about four orders of magnitude using the beamline gas cell and aluminum filters.

The DiProI experimental station (Figure 1(b)) has a flexible and adaptable design that allows detection of the diffraction pattern from objects in different configurations, fixed, or delivered by an aerosol particle injector. The performed measurements provide information about the structure and dynamics of matter with spatial and temporal resolution limited by the wavelength and duration of FERMI pulses. The main station components are an *x*-*y* sample stage for reproducible positioning of the sample with sub-micrometer precision, a photon detection system using a Charge Coupled Device (CCD), a telescope for alignment of the target position in fixed sample configuration, a time-of-flight mass spectrometer (interfaced with the CCD detector), as well as aerosol particle delivery system. Photodiodes serve as optional detection systems.

The large volume and numerous ports of the experimental chamber allow accommodation of multiple experiment configurations, including pump-probe setups. The chamber pumping system provides a vacuum environment of 10^{-7} mbar with rapid recovery after venting. Multiple apertures for beam cleaning and shaping are permanently mounted on positioning stages. Details about the construction of the measurement station and the commissioning experiments performed using synchrotron light are reported in Refs. 26 and 27.

The beam focused by the K-B mirrors enters the DiProI chamber through a 5 mm diameter circular aligning aperture and a fast shutter controls the sample exposure time, ranging from a single shot to several hundred attenuated FEL pulses in an integrative non-destructive regime. A screen with a square aperture of 500 μm side length blocks stray radiation, allowing only the focused beam to interact with the sample. The changes in the spot size on the sample plane can be monitored by Ce-YAG or phosphor scintillator using attenuated beam intensities. However, due to saturation of the scintillator at high fluence, this diagnostic is not suited for spot size estimation. A more reliable method is to measure the size of the crater ablated by a single FEL pulse in a soft material such as Poly Methyl MethAcrylate (PMMA) polymer.

After focusing a 10 μJ FEL pulse, the photon flux is well above the PMMA damage threshold.[28] From the crater, shown in Figure 1(c), created with a single pulse, we estimated that the spot size is $\sim 40 \times 50\ \mu m^2$ with an internal hot spot of $25 \times 30\ \mu m^2$. This focal spot size is still far from the designed goal of $5 \times 3\ \mu m^2$, but was sufficient for the first proof-of-principle commissioning experiments.

Diffraction patterns were measured by CCD, either in an indirect configuration (Figure 1(d)), where a multilayer mirror with a central hole reflects the scattered photons on the Princeton-CCD and the primary beam passes through the hole,[29,30] or in a direct configuration (X-CAM-CCD, Figure 1(e)) consisting of two modules separated by a central gap.[31]

III. COMMISSIONING RESULTS

The samples used in the reported measurements were chosen considering the available FERMI FEL-1 parameters and the present performance of the optical beam transport and focusing system of the DiProI beamline.[24,25] Further improvements and developments, taking into account the feedback from the first experiments and considering the stringent requirements of the broad user community, are ongoing. The aims of the commissioning experiments were (i) to verify the performance of the optics regarding the preservation of coherence, beam demagnification, and stability; (ii) to establish the conditions to enable single-shot CDI and FTH experiments using test samples of sub-10 μm dimensions; (iii) to demonstrate the advantage of circularly polarized seeded FERMI FEL pulses for imaging of magnetic domain patterns. The experiments were carried out in partnership with scientists from DESY, who provided test samples and the direct detection system in Figure 1(e).

A. FERMI FEL coherence in the focal spot

The full coherence, in which all the phases of the electromagnetic wave are correlated in space and time, is an ideal feature closely approached by optical laser and FEL radiation.[32–34] Characterization of the FEL beam coherence, before and after the beam transport and focusing optics, is essential for the CDI and FTH experiments, which require

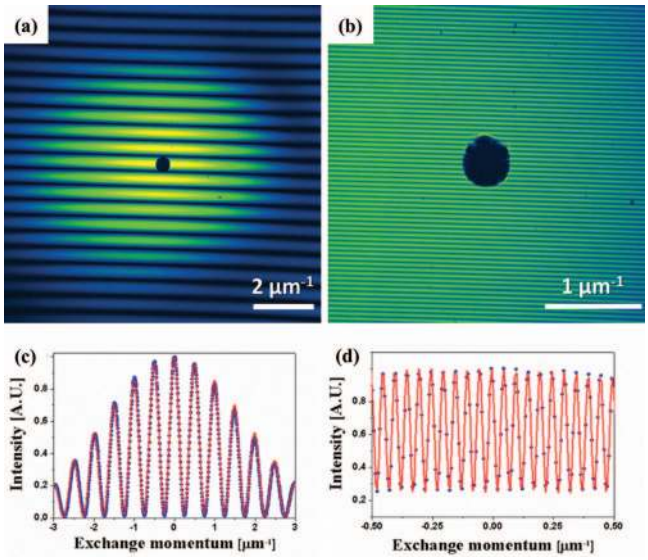

FIG. 2. (Top) Interference fringes for Young's double pinhole experiments with separation (a) 2 μm and (b) 20 μm. (Bottom) Line profiles of interference fringes (blue dots) and fit of experimental data with Eq. (1) for separation (c) 2 μm and (d) 20 μm.

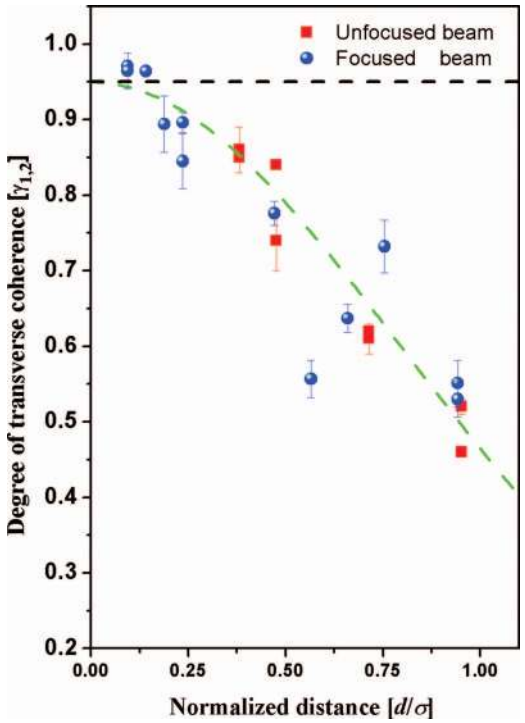

FIG. 3. Measured degree of transverse coherence at 32.5 nm as a function of the separation between the two pinholes for focused (25 μm) beam (blue circles) and unfocused beam before the K-B mirror (red squares). For the sake of comparison, the x axis shows the normalized distance separation, dividing d by the beam dimension σ. Dashed lines show the fit of the experimental data with the Gaussian Schell model considering the contribution of a single mode (black) or three modes (green).

preserved phase correlation in a beam portion having at least the size of the sample under investigation.

Usual measure for the degree of coherence is the interference contrast in the far-field diffraction pattern obtained using the classical Young's double-slit arrangement as an object.[35] Illuminating the double slit with a monochromatic point source results in a set of interference fringes and a fringe visibility of 100% corresponds to developed distinct maxima with zero intensity in the minima. Figures 2(a) and 2(b) show the patterns for two pinholes of 250 nm diameter, separated by 2 and 20 μm, recorded with the indirect detection system working with a 32.5 nm mirror. Under the Fraunhofer limit, the diffraction pattern recorded at a position P in the Young's experiment can be described by the following expression:

$$I(P) = I_1(P) + I_2(P) + \sqrt{I_1(P) \times I_2(P)} \times |\gamma_{12}(\tau)| \times \cos[\omega \times \tau - \alpha_{12}(\tau)], \quad (1)$$

where $I_1(P)$ and $I_2(P)$ are the Airy distributions due to diffraction through the two pinholes of diameter D, γ_{12} is the degree of transverse coherence, τ is the time delay for the radiation to reach point P from the different pinholes, ω is the mean frequency of the incoming radiation, and $\alpha_{12}(\tau)$ is the relative phase.

Fitting the line profiles in Figures 2(c) and 2(d) with the expression in Eq. (1), we get a degree of transverse coherence of 96 $\pm$ 2% and 55 $\pm$ 2% for the two length scales, respectively.

Figure 3 shows the dependence of the degree of transverse coherence on the pinhole separation for a set of samples. The dashed lines are simulations based on the Gaussian Schell model for weighted sum of independent modes that propagate from the source to the sample.[36] This approach was also used by Singer *et al.*[32] and Vartanyants *et al.*[33,37] to measure the degree of coherence of FLASH and the LCLS. The complex degree of coherence in this model is described as

$$\gamma(\mathbf{r_1}, \mathbf{r_2}, \tau) = \frac{\Gamma(\mathbf{r_1}, \mathbf{r_2}, \tau)}{\sqrt{I(\mathbf{r_1})} \cdot \sqrt{I(\mathbf{r_2})}}, \quad (2)$$

where $\Gamma(\boldsymbol{r_1}, \boldsymbol{r_2}, \tau)$ is the mutual coherence function of the electromagnetic field $\boldsymbol{E}(\boldsymbol{r_1}, \boldsymbol{r_2}, \tau)$, defined as $\Gamma(\boldsymbol{r_1}, \boldsymbol{r_2}, \tau) = \langle \boldsymbol{E}(\boldsymbol{r_1}, t+\tau) \cdot \boldsymbol{E}^*(\boldsymbol{r_2}, t+\tau) \rangle_T$, the brackets $\langle \ldots \rangle_T$ indicate averaging over times T, and $I(\boldsymbol{r})$ is the average intensity of the field. In the frequency domain, the mutual coherence function defines the cross-spectral density $W(\boldsymbol{r_1}, \boldsymbol{r_2}, \omega)$ of the radiation field as its Fourier transform and can be decomposed into independent Gaussian Hermite modes $E_i(\boldsymbol{r}, \omega)$ weighted by the eigenvalues β_i as

$$W(\mathbf{r_1}, \mathbf{r_2}, \omega) = \int_{-\infty}^{\infty} \Gamma(\mathbf{r_1}, \mathbf{r_2}, \tau) \cdot e^{i\omega\tau} = \sum \beta_i \cdot E_i(\mathbf{r_1}, \omega) \cdot E_i(\mathbf{r_2}, \omega). \quad (3)$$

In this approach, the wave front emitted from the source and the coherence properties on the sample plane can be calculated, considering the beam dimensions, divergence and distance from the source and assuming negligible wave-front distortion by the optics. Close inspection of the obtained results shows that the radiation field is not fully coherent, but more modes of the source contribute to the wave front impinging on the sample.

The best fit of the experimental data (green dashed line in Figure 3) requires three modes, where 55% of the energy is emitted in the first Gaussian mode, while the second and third

modes contribute by 30% and 15% to the total emitted field. For comparison, the red squares show the degree of coherence measured before the K-B focusing system at ∼70 m from the source.[22,24,25] Within the error bar they follow the same trend, which demonstrates that the degree of coherence is preserved in the focused beam.

These results show that for small objects, as the ones we used for the test experiments described below, the transverse coherence is better than 80%. In such regime the coherence of the beam is high enough to assume that the impinging radiation on the sample can be approximated to a fully coherent wave front and consequently single mode phase retrieving algorithms[38–40] can be applied to get the real space image of the scattering object. For larger samples the presence of multiple transversal modes inside the impinging wavefront imposes their independent propagation from the sample to the detector plane in the phase retrieving computational process for a successful reconstruction.[41–43]

B. Single-shot coherent imaging of test samples

The first proof-of-principle CDI experiments with fixed targets using FERMI FEL were carried out with 32.5 nm pulses using the indirect detection system as shown in Figure 1(d). The target objects were fabricated by Focused Ion Beam (FIB) depositing a 100 nm thick platinum film on $50 \times 50\ \mu m^2$ wide, 20 nm thick Si_3N_4 windows. As shown in Figures 4(a) and 4(b), around the main objects, having lateral dimensions of $5 \times 2.5\ \mu m^2$ and $7.5 \times 7.5\ \mu m^2$, respectively, three reference dots of 250 nm diameter are deposited, at the vertex of an equilateral triangle, to perform holographic imaging, as well. To guarantee sufficient contrast for the reconstruction of the image from the measured speckle pattern, the distance between the reference dots and the sample's barycenter is chosen to be 10 μm for the sample in Figure 4(a) and 15 μm in Figure 4(b), to secure that the hologram does not overlap with the autocorrelation function of the object.

Figures 4(c) and 4(d) show the diffraction pattern, measured hitting the sample with a single focused FEL pulse. For a FEL pulse energy of ∼20 μJ, the photon flux density in the focal spot on the sample is 2.6×10^9 photons/μm^2. Under such experimental conditions, the amount of energy deposited in the sample induces the evaporation of the structures due to the Coulomb explosion after the interaction with the FEL pulse. However the hydrodynamic sample expansion happens on a longer time scale (∼1–10 ps) with respect to the pulse temporal duration (<100 fs)[44,45] allowing to obtain morphological information of the illuminated sample before its destruction.[30]

Each diffraction pattern in Figures 4(c) and 4(d) contains about 1×10^8 photons and records information at the edges of the CCD plane up to a spatial frequency of 9.8 μm^{-1}, which is equivalent to diffraction limited resolution of about 50 nm. For the simple object in Figure 4(a), some structural information can be directly inferred from the analysis of the diffraction pattern. The oval diffraction modulation with a periodicity of about 0.5 μm^{-1} in Figure 4(c) corresponds to the circular ring of the object with real space dimension of about

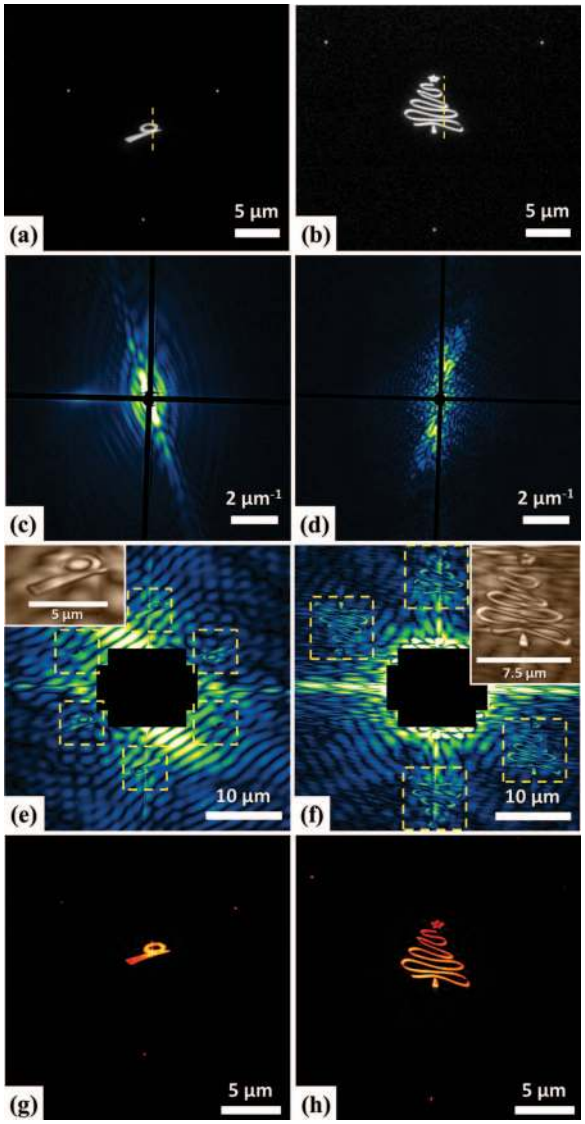

FIG. 4. (a) and (b) SEM image of the samples; profiles taken along the dashed yellow lines are shown in Figures 5(a) and 5(b). (c) and (d) Single-shot diffraction pattern with 32.5 nm FEL pulse. (e) and (f) Holographic reconstruction of the objects (dashed yellow squares highlight their positions), with one enlarged hologram in the inset. (g) and (h) Phase retrieval reconstruction.

2 μm, while the bright stripe at about 20° with respect to the vertical axis is due to the stretched triangle below the ring forming the object. For the more complex object, shown in Figure 4(b), a real space reconstruction is necessary to obtain structural information.

Inside both diffraction patterns in Figures 4(c) and 4(d), one can see a fine modulation of 0.1 μm^{-1} and 0.067 μm^{-1}, respectively, corresponding to the spatial distance between main object and reference dots. Such fine amplitude modulation encodes the relative phase between the scattering wave from the object and the reference dots, allowing fast reconstruction of the image with a single Fourier transform process of the diffraction pattern. In the obtained holograms, the reference signal is sufficiently strong to reconstruct the objects: in the first case (Figure 4(e)) six holograms of different intensities appear (two of them barely visible), while in

the second case (Figure 4(f)) only four holograms are visible. This difference can be ascribed to non-homogenous illumination of the structures in a single-shot mode, due to the hot spot in the focused beam shown in Figure 1(c). In fact its lateral dimension of 25 × 30 μm^2 is comparable to the distance (26 μm) between the dots forming the reference triangle in Figure 4(b).

The diffraction patterns in Figures 4(c) and 4(d) can also be used to reconstruct the scattering object applying phase retrieval techniques. Figures 4(g) and 4(h) show the obtained reconstruction using 2000 iterations of the Relaxed Averaged Alternating Reflections (RAAR) algorithm[40] combined with a "Shrinkwrap" dynamic support constraint[46] without any *a priori* knowledge about the object. The reconstructed image shows both the main object and the reference dots. It should be noted that, while in Figure 4(g), three dots are present, only two are visible in the reconstruction of the object in Figure 4(h), consistently with the supposed partial illumination of the sample in the last case.

For the sake of comparison of the resolution between CDI reconstructed objects and the corresponding SEM images, we show in Figures 5(a) and 5(b) the line profiles taken along the dashed yellow lines in Figures 4(a) and 4(b). The CDI reconstructed objects provide metrological information of the internal structures, retrieving both the line width (∼300 ± 25 nm) and the separation between different features, as small as ∼170 nm (marked by arrows in Figure 5(b)).

The resolution of each CDI image is estimated from the Phase Retrieval Transfer Functions (PRTFs),[30,47] where, performing 10 independent reconstructions from different starting points in the phase space, the average amplitudes in the Fourier space are compared to the amplitudes of the measured diffraction pattern. As shown in Figures 5(c) and 5(d), the resolution of both CDI images is ∼75 ± 2 nm, corresponding to the exchanged momentum for which the PRTF drops below 1/*e*.[48]

These results confirm that the intensity and temporal structure of FERMI FEL-1 pulses are sufficient to get a snapshot image of a micro object before its Coulomb-explosion and the source's spectral purity is an asset for the image reconstruction process.

C. Towards single-shot magnetic scattering

1. Resonant magnetic scattering experiments

The possibility to provide intense and ultra-short pulses with variable polarization has granted a way to probe elementary magnetization dynamics such as spin-flip and the basic process associated to energy and angular momentum transfer between the electron/spin system and the crystalline lattice. As shown by Gutt *et al.*,[49] the magnetic domains of the Co/Pt multilayer film are weakly affected by the interaction with the FEL pulse in non-destructive regime if the photon flux is kept below 4 mJ/cm^2. This enables to obtain information on the magnetic structure from the recorded X-ray scattering speckles, such as the average domain size.

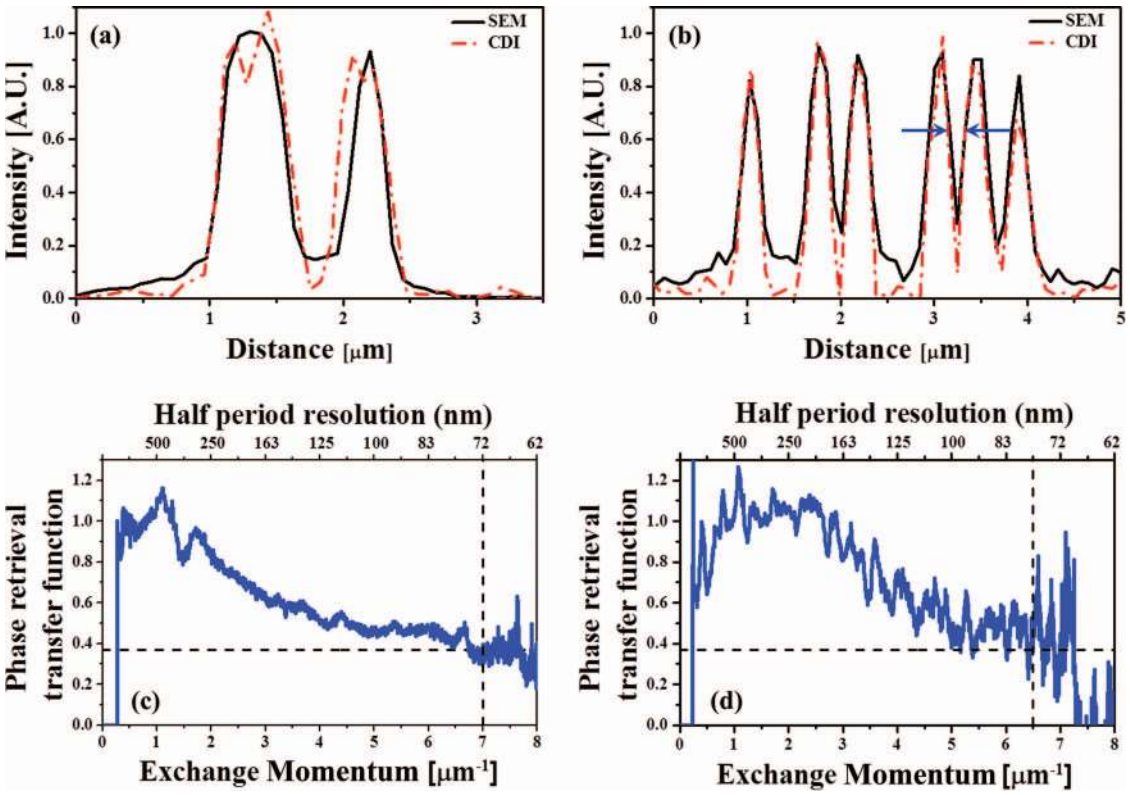

FIG. 5. (a) and (b) Profiles taken along the dashed yellow lines in the SEM images of Figures 4(a) and 4(b) and in the corresponding CDI reconstructed images (Figures 4(g) and 4(h)). (c) and (d) PRTF obtained averaging the Fourier amplitude of 10 independent reconstructions with different random phases as starting guess; the dashed lines highlight where the PRTF drop below 1/*e*.

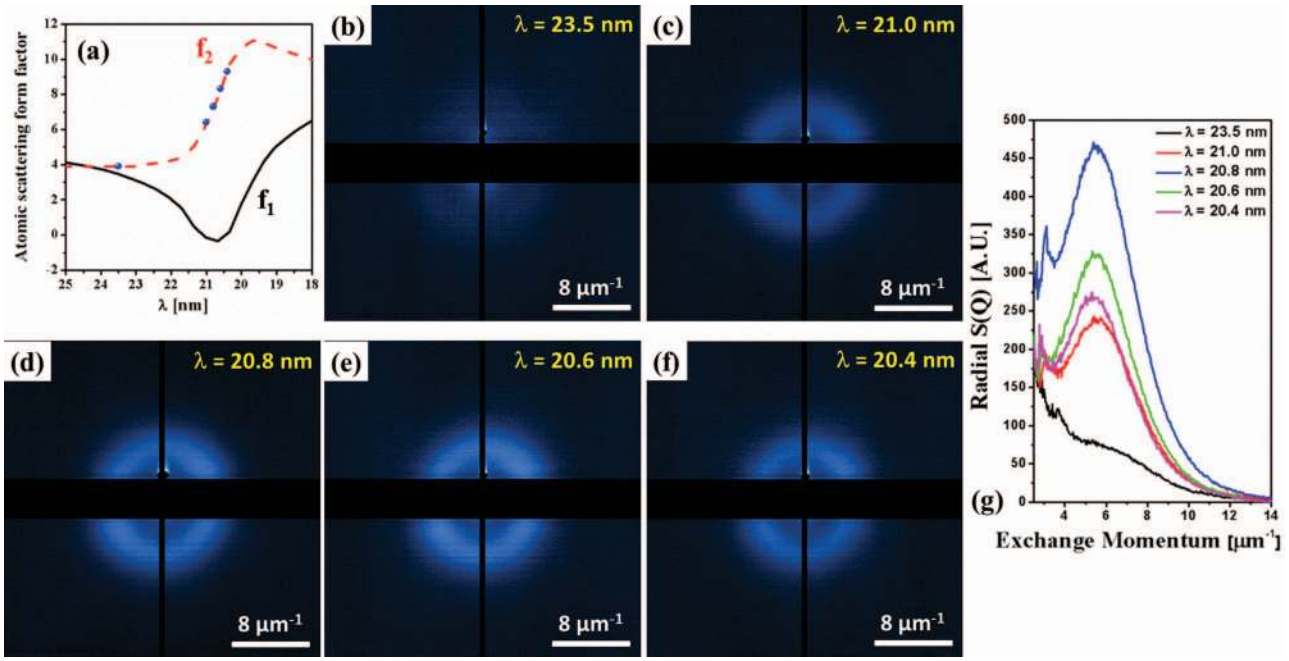

FIG. 6. (a) Atomic scattering form factor of cobalt taken from Ref. 55: dots highlight the measurement wavelengths in (b)–(f) around the resonance at the Co $M_{2,3}$-edge at 20.8 nm. (b)–(f) Scattering patterns of a Co/Pt multilayer sample at 23.5 nm, 21.0 nm, 20.8 nm, 20.6 nm, and 20.4 nm. (g) Radial average of (b)–(f) showing a maximum of magnetically scattered photons at the Co $M_{2,3}$ absorption edge (20.8 nm).

Here, we report on the opportunities opened by FERMI to perform resonant magnetic scattering experiments employing the X-ray Magnetic Circular Dichroism (XMCD) effect by fine tuning the wavelength of the FEL pulses across an absorption edge and using variable polarization.[50–52] In such experiments the scattered intensity is proportional to the square of the local domain magnetization vector **M** projected onto the propagation vector **k** of the incident circularly polarized photons. A domain pattern with alternating magnetization thus leads to a pronounced small-angle scattering signal of magnetic origin.

The samples used are ferromagnetic $(Co_{0.8nm}/Pt_{1.4nm})_{16}$ multilayer thin films with an out-of-plane easy axis of magnetization, grown via dc magnetron sputtering on a 250 $\times$ 250 μm^2 wide, 50 nm thick Si_3N_4 membrane;[53,54] an initial 5 nm thick Pt layer grown via electron-cyclotron-resonance sputtering serves as a seed layer. By an out-of-plane demagnetization or in-plane magnetization procedure, the samples can be prepared in an equilibrium maze or metastable ordered stripe domain phase, respectively. The typical domain size in both cases is of the order of 100 nm, but the equilibrium maze domain configuration yields larger domain sizes than the aligned stripe domain phase. The exact domain sizes and the difference between both states depend on details of the growth process and the later magnetic treatment of the sample.

Resonant magnetic scattering from ferromagnetic domains of Co/Pt multilayer samples has successfully been detected using the circularly polarized FERMI pulses at a wavelength of 20.8 nm, corresponding to the $M_{2,3}$-edge of cobalt. In order to work below the beam damage threshold of the magnetic film, the experiments were performed with a defocused beam with a spot size of about 250 $\times$ 250 μm^2 and attenuated FEL pulse intensity using aluminum filters. The scattered photons were measured with the X-CAM detection system as shown in Figure 1(e).

Figures 6(b)–6(f) show a set of patterns created by the photons scattered from the magnetic domains, tuning the FERMI FEL wavelength to the Co $M_{2,3}$ absorption edge, as illustrated in Figure 6(a). The measurements were performed in integration mode, summing over 30 pulses with an average pulse intensity of $\sim$1 μJ ($\sim 1.3 \times 10^{11}$ photons/pulse). The spectral purity and stability of the seeded FERMI pulses have allowed fine tuning across the Co $M_{2,3}$ absorption edge. We would like to note that, compared to FELs using fixed gap undulators, the change of the FERMI wavelength is relatively fast ($\sim$10 min). It is determined by the time required for changing the undulator gap, since the simultaneous tuning of the seed laser wavelength is automatised.[22] As shown in Figure 6, the magnetic scattering ring becomes visible when approaching the Co $M_{2,3}$ edge and the intensity reaches its maximum when the absorption is maximized (Figure 6(g)).

In Figures 6(c)–6(f) no fine speckle-like structures from the single magnetic domain are visible inside the scattering ring, because a defocused spot size of 250 μm, larger than the characteristic domain dimension ($\sim$100 nm) was adopted to reduce the FEL intensity to a low fluence regime (~ 2 mJ/cm^2) in order to optimize the scattering signal minimizing the sample damage. As a consequence, the maze pattern of the magnetic Co/Pt sample generates a scattered diffraction pattern with radial azimuthal symmetry and almost uniform intensity. However, the scattering ring provides information about the average width of the domains: we evaluated that for our sample, the maximum of the magnetic scattering intensity lies at ~ 5.75 μm^{-1}, corresponding to a magnetic periodicity of $\sim$180 nm, which implies an average domain width of $\sim$90 nm, in good agreement with the sample structure design.

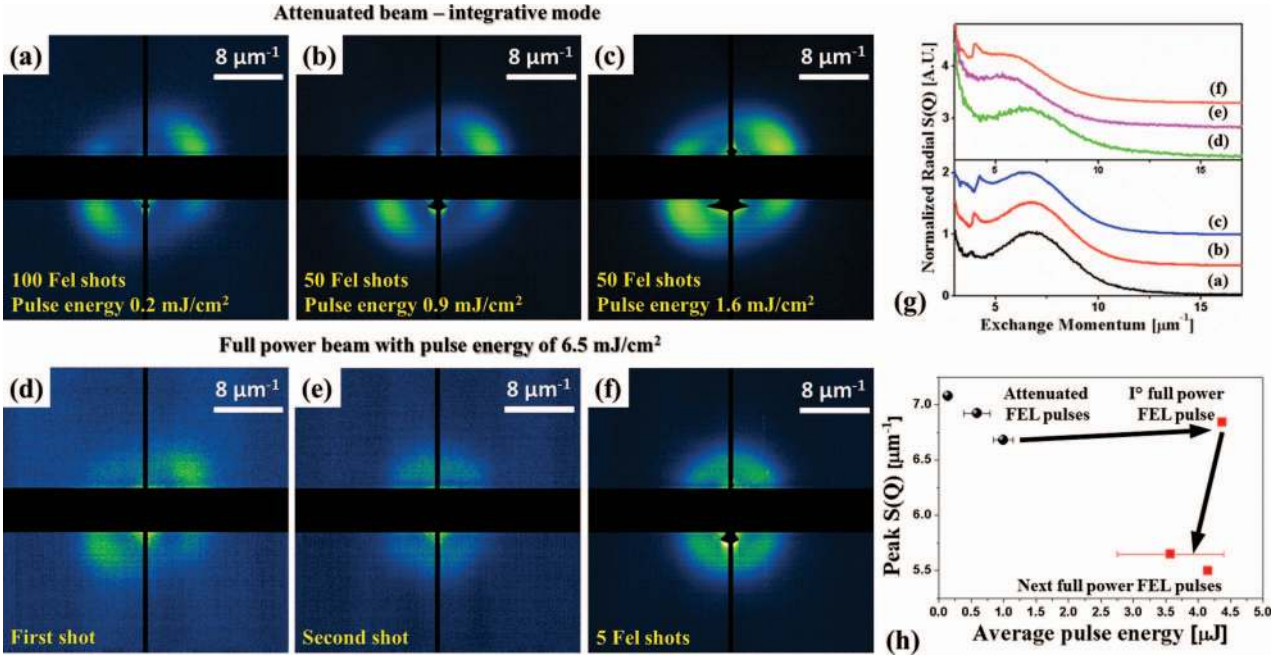

FIG. 7. (a)–(f) Magnetic scattering patterns taken with different fluences: (a) 100 pulses with average energy 0.15 μJ; (b) 50 pulses with average energy 0.6 μJ; (c) 50 pulses with average energy 1 μJ; (d) single-shot pulse of 4.3 μJ; (e) successive single-shot pulse of 4 μJ; and (f) integrative image of 5 successive pulses of ~3.5 μJ. (g) Plots of the scattering profiles obtained by azimuthally averaging intensities of images (a)–(f). (h) Dependence of the peak position of the scattering pattern on the average pulse energy.

Although it is possible to perform non-destructive measurements of magnetic thin films using a FEL source,[49] one has to keep in mind that the intense FEL pulse can drive the sample into a different state, transiently or permanently, an opportunity for dynamic studies using the ultrashort FEL pulses that are not feasible using synchrotron radiation. The case of a permanent change in the magnetic state of a sample is explored here, using a multilayer sample that was *ex situ* prepared in a metastable stripe domain phase by a 5 T external magnetic field. The resulting stripe domain pattern causes an anisotropic scattering image showing two pronounced lobes at about 20° with respect to the horizontal image axis (Figures 7(a)–7(c)). While during the acquisition of these images, the attenuated pulses do not induce any noticeable domain change, the higher fluences used to obtain single-shot patterns (Figures 7(d)–7(f)) induce a permanent modification of the sample's magnetic state.

Note that the first high-fluence single shot (Figure 7(d)) still probes the unchanged state, whereas the second shot (Figure 7(e)) shows the changes induced by the first one: the anisotropy of the scattering pattern has vanished and the ring radius moves toward lower exchanged momentum. Hence, the sample has been driven into a disordered maze domain state with no preferred domain orientation, which is the equilibrium configuration for these types of samples. Therefore, no further substantial changes occur, as evidenced by the images measured in the following shots (Figure 7(f)).

By driving the system into its equilibrium magnetic phase, a shift towards lower momentum exchange of the scattering intensity maxima is observed, which corresponds to an increase of the domain period from about 140 nm to 180 nm (Figures 7(g) and 7(h)). It is important to note that the observed changes in the magnetic scattering pattern, which are induced by the FEL pulses, do not constitute an ultrafast phenomenon, but are caused by sample heating.[49]

2. Fourier transform holography at the Co $M_{2,3}$-edge

Apart from the single-shot CDI experiments, the ability of FERMI FELs to deliver fully circularly polarized pulses, has opened a unique opportunity for single-shot magnetic imaging experiments on the nanoscale, employing the FTH scheme.[14,56] FTH of magnetic materials requires circularly polarized light, since the linearly polarized one is not an eigenstate of magnetic scattering and therefore magnetically scattered radiation from the object hole cannot interfere with charge scattered radiation from the references.[57] While the feasibility of single-shot FTH at an FEL source was previously shown by employing a transmission polarizer to produce elliptically polarized light,[58,59] this approach has the drawback of a loss of almost two orders of magnitude in intensity and only 60% of circular polarization.

The concept of transmission polarizer cannot be easily extended at longer wavelength due to the stronger material adsorption in the VUV region. To produce FEL pulses with circular polarization, FERMI uses instead APPLE-II type undulators, which in a synchrotron based seeded FEL have produced circularly polarized light with a measured degree of polarization between 85% and 95%.[60] Taking into account the optical layout of the DiProI beam-line, the difference in the VUV mirrors reflectivity of *s* and *p* wave components has negligible influence on the source polarization at 20.8 nm: we estimate that the transmission of the beamline mirror system affects the source polarization by less than 5%.

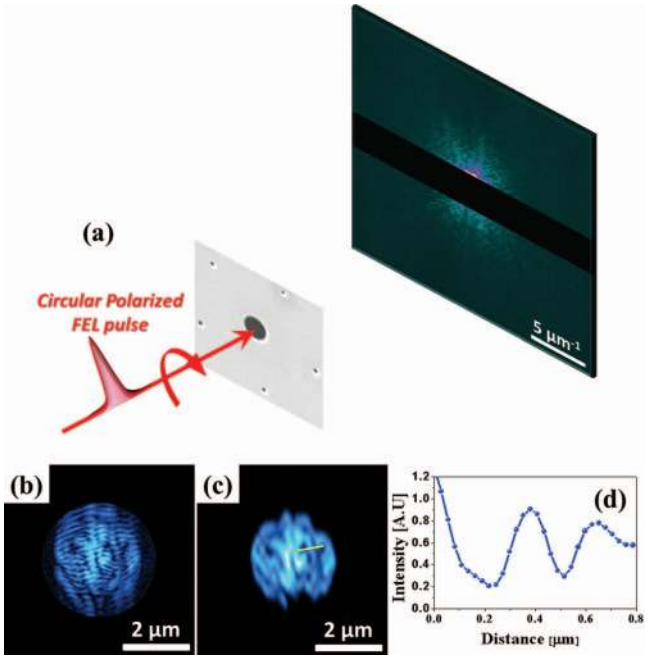

FIG. 8. (a) Experimental setup. Scanning electron microscopy image of the 5-references holography mask: the sample aperture is 2.5 μm and the references 100 nm. A single-shot spectro-hologram is acquired on a CCD camera located at 48 mm downstream. (b) Reconstructed hologram of the magnetic structure using the diffraction pattern in (a): dark and bright regions are domains with opposite out-of-plane magnetization directions. (c) CDI reconstruction of the magnetic structure, using image (b) as starting guess in RAAR phase retrieving algorithm. (d) Intensity profile along the yellow line in (c).

Using the polarized FERMI pulses, it was possible to record a magnetic hologram with a single 20.8 nm 80–100 fs pulse with energy ~30 mJ/cm^2, focused to a 50 × 50 μm^2 spot on the sample. Figure 8(a) shows the first single-shot magnetic holography image recorded at the Co $M_{2,3}$-edge using a circularly polarized FEL pulse. A 5-reference holographic mask, consisting of a field of view aperture of 2.5 μm diameter, surrounded at 6.25 μm by 5 reference pin-holes of 100 nm diameter, was placed in close contact to a magnetic multilayer Co/Pt film described in Sec. III C 1.

The bright and dark stripes in the reconstructed image in Figure 8(b) are representing the magnetic domains pointing in up and down directions perpendicular to the sample surface. Due to the 2 mm gap of the X-CAM detector, the central part of the hologram is missing which accounts for the artifacts in the reconstructed image, i.e., the horizontal short-period modulation. By applying 2000 iterations of RAAR phase retrieval algorithm, using the image in Figure 8(b) as a starting guess, the image quality can be improved and the influence of the artifacts minimized (Figure 8(c)).

Figure 8(c) confirms that the system is in the stripe domain phase, that was prepared applying an external in-plane magnetic field to the multilayer system after sample preparation. In the reconstructed image the stripes are aligned at about 20°, in good agreement with the angle inferred on the same sample in the unmasked scattering experiments (Figures 7(a)–7(c)). Figure 8(d) shows an intensity line scan through the reconstructed image which reveals the typical magnetic domain size of ~100 nm.

We would like to notify that the relatively low image quality, compared with similar experiments performed at L edges with synchrotrons and LCLS[14,59] is due to several factors: (i) the XMCD contrast at L-edges is 2-3 times higher than that at the M-edges used here;[61] (ii) the ultimate CDI spatial resolution is higher at shorter wavelengths and (iii) the total cross sections for Co ionization are higher at our longer wavelengths, which means that the "magnetic scattering intensity quenching"[62] induced by the propagation of the intense FEL pulse inside the material in single-shot experiments is more pronounced in our case. The planned shortening the FERMI pulse duration to less than 50 fs will reduce the effect of the X-ray damage and, beyond this, the contrast in magnetic single-shot femtosecond X-ray FTH can be increased in future experiments by making use of extended reference structures such as lines or triangles in the holographic mask.[13]

However, certain advantage using the M-edges is provided by the higher scattering intensity, which is an important factor for the future time-resolved experiments, which cannot be carried out in the integration mode, used at the synchrotron facilities. The jitter-free optical pumping, available at FERMI using the naturally triggered seed laser, will enable time resolved stroboscopic imaging of magnetic domains in the non-equilibrium state. One application will be to elucidate the recently found super-diffusive spin-transport across the ferromagnetic-ferromagnetic domain walls during ultrafast demagnetization.[63]

IV. CONCLUSIONS AND OUTLOOK

The first commissioning results presented here demonstrate the potential of FERMI@Elettra seeded FEL for efficient CDI, FTH and resonant magnetic CDI experiments with fixed targets in integrative and single-shot modes. The main advantage using seeded FERMI FEL-1 is in resonant CDI, where the tunable, stable and narrow bandwidth of FERMI pulses with controlled linear or circular polarization opens unprecedented opportunities to explore multicomponent nanostructures in equilibrium or transient states, in order to access spatial aspects in dynamic processes. The ongoing commissioning of the FERMI FEL-2 will provide 4 nm wavelength pulses in the first harmonic in 2013. Expanding the wavelength range to even shorter wavelengths will increase the number of the reachable atomic resonances, enabling resonant CDI at the K-edge of carbon in the first harmonic and at the K and L-edges of many elements in the higher harmonics of the radiation (e.g., the 3d transition metals) and pushing the wavelength-limited resolution as well. Indeed, using soft X-rays the CDI spatial resolution will be limited to 5–10 nm and cannot compete with the sub-nm resolution that can be achieved using hard X-rays but the transient events and in many non-periodic systems occur at space scales achievable by the soft X-rays. In fact, the much stronger interactions of soft X-rays with matter results in stronger scattered signal, which has been demonstrated[64] to be of particular importance for imaging of soft matter and biological objects in their native state, e.g., in the water window between the oxygen and carbon K-edges.

In 2013, the optical laser pumping is implemented by using the FERMI seed laser. This is a great advantage compared to the pumping schemes using external optical laser since the seed laser is naturally triggered with the FERMI pulses and allows performing jitter-free pump-probe experiments which has been considered as a major advantage of high harmonic generation laboratory sources. Another possible time resolved experiments will be FEL-pump FEL-probe approach using a split-delay line or two color FEL pulses generated by the same electron bunch. The latter is another advantage of seeded FEL using external laser: development and implementation of specific seeding schemes to produce two or more pulses split in time and energy.[65,66] These new approaches will enable various types of time resolved experiments with temporal resolution in the femtosecond to nanosecond range opens for exploring dynamic phenomena triggered by excitations with ultra-short VUV-soft X-ray pulses.

ACKNOWLEDGMENTS

The authors thank the FERMI commissioning team for their assistance and cooperation and are particularly grateful to E. Allaria, F. Bencivenga, W. Fawley and C. Spezzani for the illuminating discussions. We thank G. Winkler, M. Hille, M. Rahbar Azad and B. Beyersdorff from Hamburg University for the preparation of samples for magnetic scattering experiments.

This work was funded by the FERMI project of Elettra-Sincrotrone Trieste, partially supported by the Italian Ministry of University and Research under Grant Nos. FIRB-RBAP045JF2 and FIRB-RBAP06AWK3. S.S., L.M., C.G. and G.G. would like to gratefully acknowledge support from the DFG within SFB925 and SFB668, the Clusters of Excellence "Frontiers in Quantum Photon Science" and "Nano-Spintronics", and the BMBF under Contract No. 05K10GU4/FSP-301.

[1] A. Sakdinawat and D. Attwood, Nat. Photonics **4**, 840 (2010).
[2] B. Kaulich, P. Thibault, A. Gianoncelli, and M. Kiskinova, J. Phys.: Condens. Matter **23**, 083002 (2011).
[3] R. Falcone, C. Jacobsen, J. Kirz, S. Marchesini, D. Shapiro, and J. Spence, Contemp. Phys. **52**, 293 (2011).
[4] J. Miao, P. Charalambous, J. Kirz, and D. Sayre, Nature (London) **400**, 342 (1999).
[5] K. A. Nugent, Adv. Phys. **59**, 1 (2010).
[6] H. N. Chapman and K. A. Nugent, Nat. Photonics **4**, 833 (2010).
[7] K. J. Gaffney and H. N. Chapman, Science **316**, 1444 (2007).
[8] C. Song, R. Bergstrom, D. Ramunno-Johnson, H. Jiang, D. Paterson, M. de Jonge, I. McNulty, J. Lee, K. Wang, and J. Miao, Phys. Rev. Lett. **100**, 025504 (2008).
[9] A. Scherz, D. Zhu, R. Rick, W. Schlotter, S. Roy, J. Lüning, and J. Stöhr, Phys. Rev. Lett. **101**, 076101 (2008).
[10] A. Tripathi, J. Mohanty, S. H. Dietze, O. G. Shpyrko, E. Shipton, E. E. Fullerton, S. S. Kim, and I. McNulty, Proc. Natl. Acad. Sci. U.S.A. **108**, 13393 (2011).
[11] R. L. Sandberg, C. Song, P. W. Wachulak, D. A. Raymondson, A. Paul, B. Amirbekian, E. Lee, A. E. Sakdinawat, C. La-O-Vorakiat, M. C. Marconi, C. S. Menoni, M. M. Murnane, J. J. Rocca, H. C. Kapteyn, and J. Miao, Proc. Natl. Acad. Sci. U.S.A. **105**, 24 (2008).
[12] A. Ravasio, D. Gauthier, F. R. N. C. Maia, M. Billon, J.-P. Caumes, D. Garzella, M. Géléoc, O. Gobert, J.-F. Hergott, A.-M. Pena, H. Perez, B. Carré, E. Bourhis, J. Gierak, A. Madouri, D. Mailly, B. Schiedt, M. Fajardo, J. Gautier, P. Zeitoun, P. H. Bucksbaum, J. Hajdu, and H. Merdji, Phys. Rev. Lett. **103**, 028104 (2009).
[13] D. Gauthier, M. Guizar-Sicairos, X. Ge, W. Boutu, B. Carré, J. R. Fienup, and H. Merdji, Phys. Rev. Lett. **105**, 093901 (2010).
[14] S. Eisebitt, J. Lüning, W. F. Schlotter, M. Lörgen, O. Hellwig, W. Eberhardt, and J. Stöhr, Nature (London) **432**, 885 (2004).
[15] R. Neutze and J. Hajdu, Proc. Natl. Acad. Sci. U.S.A. **94**, 5651 (1997).
[16] H. N. Chapman, Nature Mater. **8**, 299 (2009).
[17] A. Barty, S. Boutet, M. J. Bogan, S. Hau-Riege, S. Marchesini, K. Sokolowski-Tinten, N. Stojanovic, R. Tobey, H. Ehrke, A. Cavalleri, S. Düsterer, M. Frank, S. Bajt, B. W. Woods, M. M. Seibert, J. Hajdu, R. Treusch, and H. N. Chapman, Nat. Photonics **2**, 415 (2008).
[18] J. Feldhaus, J. Phys. B **43**, 194002 (2010).
[19] P. Emma, R. Akre, J. Arthur, R. Bionta, C. Bostedt, J. Bozek, A. Brachmann, P. Bucksbaum, R. Coffee, F.-J. Decker, Y. Ding, D. Dowell, S. Edstrom, A. Fisher, J. Frisch, S. Gilevich, J. Hastings, G. Hays, P. Hering, Z. Huang, R. Iverson, H. Loos, M. Messerschmidt, A. Miahnahri, S. Moeller, H.-D. Nuhn, G. Pile, D. Ratner, J. Rzepiela, D. Schultz, T. Smith, P. Stefan, H. Tompkins, J. Turner, J. Welch, W. White, J. Wu, G. Yocky, and J. Galayda, Nat. Photonics **4**, 641 (2010).
[20] T. Ishikawa, H. Aoyagi, T. Asaka, Y. Asano, N. Azumi, T. Bizen, H. Ego, K. Fukami, T. Fukui, Y. Furukawa, S. Goto, H. Hanaki, T. Hara, T. Hasegawa, T. Hatsui, A. Higashiya, T. Hirono, N. Hosoda, M. Ishii, T. Inagaki, Y. Inubushi, T. Itoga, Y. Joti, M. Kago, T. Kameshima, H. Kimura, Y. Kirihara, A. Kiyomichi, T. Kobayashi, C. Kondo, T. Kudo, H. Maesaka, X. M. Maréchal, T. Masuda, S. Matsubara, T. Matsumoto, T. Matsushita, S. Matsui, M. Nagasono, N. Nariyama, H. Ohashi, T. Ohata, T. Ohshima, S. Ono, Y. Otake, C. Saji, T. Sakurai, T. Sato, K. Sawada, T. Seike, K. Shirasawa, T. Sugimoto, S. Suzuki, S. Takahashi, H. Takebe, K. Takeshita, K. Tamasaku, H. Tanaka, R. Tanaka, T. Tanaka, T. Togashi, K. Togawa, A. Tokuhisa, H. Tomizawa, K. Tono, S. Wu, M. Yabashi, M. Yamaga, A. Yamashita, K. Yanagida, C. Zhang, T. Shintake, H. Kitamura, and N. Kumagai, Nat. Photonics **6**, 540 (2012).
[21] J. Amann, W. Berg, V. Blank, F.-J. Decker, Y. Ding, P. Emma, Y. Feng, J. Frisch, D. Fritz, J. Hastings, Z. Huang, J. Krzywinski, R. Lindberg, H. Loos, A. Lutman, H.-D. Nuhn, D. Ratner, J. Rzepiela, D. Shu, Y. Shvyd'ko, S. Spampinati, S. Stoupin, S. Terentyev, E. Trakhtenberg, D. Walz, J. Welch, J. Wu, A. Zholents, and D. Zhu, Nat. Photonics **6**, 693 (2012).
[22] E. Allaria, A. Battistoni, F. Bencivenga, R. Borghes, C. Callegari, F. Capotondi, D. Castronovo, P. Cinquegrana, D. Cocco, M. Coreno, P. Craievich, R. Cucini, F. D'Amico, M. B. Danailov, A. Demidovich, G. De Ninno, A. Di Cicco, S. Di Fonzo, M. Di Fraia, S. Di Mitri, B. Diviacco, W. M. Fawley, E. Ferrari, A. Filipponi, L. Froehlich, A. Gessini, E. Giangrisostomi, L. Giannessi, D. Giuressi, C. Grazioli, R. Gunnella, R. Ivanov, B. Mahieu, N. Mahne, C. Masciovecchio, I. P. Nikolov, G. Passos, E. Pedersoli, G. Penco, E. Principi, L. Raimondi, R. Sergo, P. Sigalotti, C. Spezzani, C. Svetina, M. Trovò, and M. Zangrando, New J. Phys. **14**, 113009 (2012).
[23] E. Allaria, R. Appio, L. Badano, W. A. Barletta, S. Bassanese, S. G. Biedron, A. Borga, E. Busetto, D. Castronovo, P. Cinquegrana, S. Cleva, D. Cocco, M. Cornacchia, P. Craievich, I. Cudin, G. D'Auria, M. D. Forno, M. B. Danailov, R. D. Monte, G. D. Ninno, P. Delgiusto, A. Demidovich, S. D. Mitri, B. Diviacco, A. Fabris, R. Fabris, W. Fawley, M. Ferianis, E. Ferrari, S. Ferry, L. Froehlich, P. Furlan, G. Gaio, F. Gelmetti, L. Giannessi, M. Giannini, R. Gobessi, R. Ivanov, E. Karantzoulis, M. Lonza, A. Lutman, B. Mahieu, M. Milloch, S. V. Milton, M. Musardo, I. Nikolov, S. Noe, F. Parmigiani, G. Penco, M. Petronio, L. Pivetta, M. Predonzani, F. Rossi, L. Rumiz, A. Salom, C. Scafuri, C. Serpico, P. Sigalotti, S. Spampinati, C. Spezzani, M. Svandrlik, C. Svetina, S. Tazzari, M. Trovo, R. Umer, A. Vascotto, M. Veronese, R. Visintini, M. Zaccaria, D. Zangrando, and M. Zangrando, Nat. Photonics **6**, 699 (2012).
[24] D. Cocco, A. Abrami, A. Bianco, I. Cudin, C. Fava, D. Giuressi, R. Godnig, F. Parmigiani, L. Rumiz, R. Sergo, C. Svetina, and M. Zangrando, Proc. SPIE **7361**, 736106 (2009).
[25] M. Zangrando, A. Abrami, D. Bacescu, I. Cudin, C. Fava, F. Frassetto, A. Galimberti, R. Godnig, D. Giuressi, L. Poletto, L. Rumiz, R. Sergo, C. Svetina, and D. Cocco, Rev. Sci. Instrum. **80**, 113110 (2009).
[26] E. Pedersoli, F. Capotondi, D. Cocco, M. Zangrando, B. Kaulich, R. H. Menk, A. Locatelli, T. O. Mentes, C. Spezzani, G. Sandrin, D. M. Bacescu, M. Kiskinova, S. Bajt, M. Barthelmess, A. Barty, J. Schulz, L. Gumprecht, H. N. Chapman, A. J. Nelson, M. Frank, M. J. Pivovaroff, B. W. Woods, M. J. Bogan, and J. Hajdu, Rev. Sci. Instrum. **82**, 043711 (2011).
[27] F. Capotondi, E. Pedersoli, M. Kiskinova, A. V. Martin, M. Barthelmess, and H. N. Chapman, Opt. Express **20**, 25152 (2012).
[28] J. Chalupský, L. Juha, J. Kuba, J. Cihelka, V. Hájková, S. Koptyaev, J. Krása, A. Velyhan, M. Bergh, C. Caleman, J. Hajdu, R. M. Bionta, H. Chapman, S. P. Hau-Riege, R. A. London, M. Jurek, J. Krzywinski, R. Nietubyc,

J. B. Pelka, R. Sobierajski, J. Meyer-ter-Vehn, A. Tronnier, K. Sokolowski-Tinten, N. Stojanovic, K. Tiedtke, S. Toleikis, T. Tschentscher, H. Wabnitz, and U. Zastrau, Opt. Express **15**, 6036 (2007).
[29]S. Bajt, H. N. Chapman, E. A. Spiller, J. B. Alameda, B. W. Woods, M. Frank, M. J. Bogan, A. Barty, S. Boutet, S. Marchesini, S. P. Hau-Riege, J. Hajdu, and D. Shapiro, Appl. Opt. **47**, 1673 (2008).
[30]H. N. Chapman, A. Barty, M. J. Bogan, S. Boutet, M. Frank, S. P. Hau-Riege, S. Marchesini, B. W. Woods, S. Bajt, W. H. Benner, R. A. London, E. Plönjes, M. Kuhlmann, R. Treusch, S. Düsterer, T. Tschentscher, J. R. Schneider, E. Spiller, T. Möller, C. Bostedt, M. Hoener, D. A. Shapiro, K. O. Hodgson, D. van der Spoel, F. Burmeister, M. Bergh, C. Caleman, G. Huldt, M. M. Seibert, F. R. N. C. Maia, R. W. Lee, A. Szöke, N. Timneanu, and J. Hajdu, Nat. Phys. **2**, 839 (2006).
[31]See http://www.xcam.co.uk/documents/DESY_XFEL_Poster.pdf, 2009, for information about the detector system.
[32]A. Singer, I. A. Vartanyants, M. Kuhlmann, S. Duesterer, R. Treusch, and J. Feldhaus, Phys. Rev. Lett. **101**, 254801 (2008).
[33]I. A. Vartanyants, A. Singer, A. P. Mancuso, O. M. Yefanov, A. Sakdinawat, Y. Liu, E. Bang, G. J. Williams, G. Cadenazzi, B. Abbey, H. Sinn, D. Attwood, K. A. Nugent, E. Weckert, T. Wang, D. Zhu, B. Wu, C. Graves, A. Scherz, J. J. Turner, W. F. Schlotter, M. Messerschmidt, J. Lüning, Y. Acremann, P. Heimann, D. C. Mancini, V. Joshi, J. Krzywinski, R. Soufli, M. Fernandez-Perea, S. Hau-Riege, A. G. Peele, Y. Feng, O. Krupin, S. Moeller, and W. Wurth, Phys. Rev. Lett. **107**, 144801 (2011).
[34]C. Gutt, P. Wochner, B. Fischer, H. Conrad, M. Castro-Colin, S. Lee, F. Lehmkühler, I. Steinke, M. Sprung, W. Roseker, D. Zhu, H. Lemke, S. Bogle, P. H. Fuoss, G. B. Stephenson, M. Cammarata, D. M. Fritz, A. Robert, and G. Grübel, Phys. Rev. Lett. **108**, 024801 (2012).
[35]T. Young, Philos. Trans. R. Soc. London **94**, 1 (1804).
[36]L. Mandel and E. Wolf, *Optical Coherence and Quantum Optics* (Cambridge University Press, 1995).
[37]I. A. Vartanyants and A. Singer, New J. Phys. **12**, 035004 (2010).
[38]R. Gerchberg and W. Saxton, Optik **35**, 237 (1972).
[39]J. R. Fienup, Appl. Opt. **21**, 2758 (1982).
[40]S. Marchesini, Rev. Sci. Instrum. **78**, 011301 (2007).
[41]C. Q. Tran, G. J. Williams, A. Roberts, S. Flewett, A. G. Peele, D. Paterson, M. D. de Jonge, and K. A. Nugent, Phys. Rev. Lett. **98**, 224801 (2007).
[42]L. W. Whitehead, G. J. Williams, H. M. Quiney, D. J. Vine, R. A. Dilanian, S. Flewett, K. A. Nugent, A. G. Peele, E. Balaur, and I. McNulty, Phys. Rev. Lett. **103**, 243902 (2009).
[43]B. Abbey, L. W. Whitehead, H. M. Quiney, D. J. Vine, G. A. Cadenazzi, C. A. Henderson, K. A. Nugent, E. Balaur, C. T. Putkunz, A. G. Peele, G. J. Williams, and I. McNulty, Nat. Photonics **5**, 420 (2011).
[44]S. P. Hau-Riege, S. Boutet, A. Barty, S. Bajt, M. J. Bogan, M. Frank, J. Andreasson, B. Iwan, M. M. Seibert, J. Hajdu, A. Sakdinawat, J. Schulz, R. Treusch, and H. N. Chapman, Phys. Rev. Lett. **104**, 064801 (2010).
[45]H. N. Chapman, S. P. Hau-Riege, M. J. Bogan, S. Bajt, A. Barty, S. Boutet, S. Marchesini, M. Frank, B. W. Woods, W. H. Benner, R. A. London, U. Rohner, A. Szöke, E. Spiller, T. Möller, C. Bostedt, D. A. Shapiro, M. Kuhlmann, R. Treusch, E. Plönjes, F. Burmeister, M. Bergh, C. Caleman, G. Huldt, M. M. Seibert, and J. Hajdu, Nature (London) **448**, 676 (2007).
[46]S. Marchesini, H. He, H. N. Chapman, S. P. Hau-Riege, A. Noy, M. R. Howells, U. Weierstall, and J. C. H. Spence, Phys. Rev. B **68**, 140101 (2003).
[47]H. N. Chapman, A. Barty, S. Marchesini, A. Noy, S. P. Hau-Riege, C. Cui, M. R. Howells, R. Rosen, H. He, J. C. H. Spence, U. Weierstall, T. Beetz, C. Jacobsen, and D. Shapiro, J. Opt. Soc. Am. A **23**, 1179 (2006).
[48]D. Shapiro, P. Thibault, T. Beetz, V. Elser, M. Howells, C. Jacobsen, J. Kirz, E. Lima, H. Miao, and A. M. Neiman, Proc. Natl. Acad. Sci. U.S.A. **102**, 15343 (2005).
[49]C. Gutt, S. Streit-Nierobisch, L.-M. Stadler, B. Pfau, C. M. Günther, R. Könnecke, R. Frömter, A. Kobs, D. Stickler, H. P. Oepen, R. R. Fäustlin, R. Treusch, J. Feldhaus, E. Weckert, I. A. Vartanyants, M. Grunze, A. Rosenhahn, T. Wilhein, S. Eisebitt, and G. Grübel, Phys. Rev. B **81**, 100401 (2010).
[50]J. P. Hannon, G. T. Trammell, M. Blume, and D. Gibbs, Phys. Rev. Lett. **61**, 1245 (1988).
[51]J. B. Kortright, S.-K. Kim, G. P. Denbeaux, G. Zeltzer, K. Takano, and E. E. Fullerton, Phys. Rev. B **64**, 092401 (2001).
[52]C. Gutt, L.-M. Stadler, S. Streit-Nierobisch, A. P. Mancuso, A. Schropp, B. Pfau, C. M. Günther, R. Könnecke, J. Gulden, B. Reime, J. Feldhaus, E. Weckert, I. A. Vartanyants, O. Hellwig, F. Staier, R. Barth, M. Grunze, A. Rosenhahn, D. Stickler, H. Stillrich, R. Frömter, H. P. Oepen, M. Martins, T. Nisius, T. Wilhein, B. Faatz, N. Guerassimova, K. Honkavaara, V. Kocharyan, R. Treusch, E. Saldin, S. Schreiber, E. A. Schneidmiller, M. V. Yurkov, S. Eisebitt, and G. Grübel, Phys. Rev. B **79**, 212406 (2009).
[53]H. Stillrich, C. Menk, R. Frömter, and H. P. Oepen, J. Magn. Magn. Mater. **322**, 1353 (2010).
[54]M. Wellhöfer, M. Weißenborn, R. Anton, S. Pütter, and H. Peter Oepen, J. Magn. Magn. Mater. **292**, 345 (2005).
[55]See http://henke.lbl.gov/optical_constants/asf.html, 2012 as the source of reported data.
[56]S. Streit-Nierobisch, D. Stickler, C. Gutt, L.-M. Stadler, H. Stillrich, C. Menk, R. Frömter, C. Tieg, O. Leupold, H. P. Oepen, and G. Grübel, J. Appl. Phys. **106**, 083909 (2009).
[57]S. Eisebitt, M. Lörgen, W. Eberhardt, J. Lüning, and J. Stöhr, Appl. Phys. A **80**, 921 (2005).
[58]B. Pfau, C. M. Günther, R. Könnecke, E. Guehrs, O. Hellwig, W. F. Schlotter, and S. Eisebitt, Opt. Express **18**, 13608 (2010).
[59]T. Wang, D. Zhu, B. Wu, C. Graves, S. Schaffert, T. Rander, L. Müller, B. Vodungbo, C. Baumier, D. Bernstein, B. Bräuer, V. Cros, S. de Jong, R. Delaunay, A. Fognini, R. Kukreja, S. Lee, V. López-Flores, J. Mohanty, B. Pfau, H. Popescu, M. Sacchi, A. Sardinha, F. Sirotti, P. Zeitoun, M. Messerschmidt, J. Turner, W. Schlotter, O. Hellwig, R. Mattana, N. Jaouen, F. Fortuna, Y. Acremann, C. Gutt, H. Dürr, E. Beaurepaire, C. Boeglin, S. Eisebitt, G. Grübel, J. Lüning, J. Stöhr, and A. Scherz, Phys. Rev. Lett. **108**, 267403 (2012).
[60]C. Spezzani, E. Allaria, M. Coreno, B. Diviacco, E. Ferrari, G. Geloni, E. Karantzoulis, B. Mahieu, M. Vento, and G. De Ninno, Phys. Rev. Lett. **107**, 084801 (2011).
[61]C. T. Chen, Y. U. Idzerda, H.-J. Lin, N. V. Smith, G. Meigs, E. Chaban, G. H. Ho, E. Pellegrin, and F. Sette, Phys. Rev. Lett. **75**, 152 (1995).
[62]L. Müller, "Breakdown of the X-ray resonant magnetic scattering signal during pulses of XUV FEL radiation" (unpublished).
[63]B. Pfau, S. Schaffert, L. Müller, C. Gutt, A. Al-Shemmary, F. Büttner, R. Delaunay, S. Düsterer, S. Flewett, R. Frömter, J. Geilhufe, E. Guehrs, C. M. Günther, R. Hawaldar, M. Hille, N. Jaouen, A. Kobs, K. Li, J. Mohanty, H. Redlin, W. F. Schlotter, D. Stickler, R. Treusch, B. Vodungbo, M. Kläui, H. P. Oepen, J. Lüning, G. Grübel, and S. Eisebitt, Nat. Commun. **3**, 1100 (2012).
[64]M. M. Seibert, S. Boutet, M. Svenda, T. Ekeberg, F. R. N. C. Maia, M. J. Bogan, N. Tîmneanu, A. Barty, S. Hau-Riege, C. Caleman, M. Frank, H. Benner, J. Y. Lee, S. Marchesini, J. W. Shaevitz, D. A. Fletcher, S. Bajt, I. Andersson, H. N. Chapman, and J. Hajdu, J. Phys. B **43**, 194015 (2010).
[65]G. De Ninno, B. Mahieu, E. Allaria, L. Giannessi, and S. Spampinati, Phys. Rev. Lett. **110**, 064801 (2013).
[66]E. Allaria, F. Bencivenga, F. Capotondi, H. N. Chapman, M. B. Danailov, G. De Ninno, A. Demidovich, S. Di Mitri, B. Diviacco, D. Fausti, W. M. Fawley, M. Ferianis, E. Ferrari, L. V. Froehlich, A. Gessini, L. Giannessi, R. K. Ivanov, M. Kiskinova, B. Mahieu, N. Mahne, I. P. Nikolov, C. Masciovecchio, E. Pedersoli, P. Charalambous, G. Penco, L. Raimondi, P. Sigalotti, S. Spampinati, C. Spezzani, C. Svetina, M. Trovò, and M. Zangrando, "Two-color pump-probe experiment with twin-pulse-seed XUV free electron laser" (unpublished).